New Correlation for the Capture Cross Section in High-Gradient Magnetic Separation

Armin D. Ebner and James A. Ritter
Dept. of Chemical Engineering, Swearingen Engineering Center, University of South Carolina, Columbia, SC 29208

A new correlation between the capture cross-section parameter (λ) and principal variables involved in high-gradient magnetic separation (HGMS) was developed. It is based on the use of an alternative dimensionless parameter, β, in lieu of the traditional U_m/U_o, which facilitated the estimation of λ over a much broader spectrum of variables. This new correlation is far more versatile than correlations and approximate models in the current literature, which are only applicable to specific situations in HGMS systems. Overall, this new correlation should be extremely useful in the design, development, optimization and modeling of HGMS systems.

Introduction

High-gradient magnetic separation (HGMS) is a technique that has been specially designed for the removal and separation of paramagnetic particles of sizes that range between 0.1 and 50 μm. The technique is based on the use of small magnetic elements (such as stainless-steel wool or wire) that generate gradients in a uniform magnetic field. These gradients give rise to large attractive forces that allow for the removal of particles from aqueous solutions that are impossible to remove by other traditional magnetic separation methods. An HGMS unit normally consists of a canister inserted within the bore of an electromagnet, in which the magnetic element is placed. With the field turned on, a solution containing the particles is passed through the matrix until saturation, after which, the field is turned off and the material retained is collected by backflushing, which prepares the canister for the next cycle.

Theoretical and experimental attention has been paid mostly to the retention dynamics in a flowthrough HGMS bed for different configurations among the field, flow, and collector wires (Avens, 1996; Avens et al., 1992; Birss et al., 1978, 1976; Cowen and Friedlaender, 1977; Cowen et al., 1976; Cummings et al., 1976; Friedlaender et al., 1981a,b, 1978; Gerber et al., 1996, 1983; Gerber, 1994, 1984, 1980; Gerber and Lawson, 1989; Gerber and Birss, 1983; Iacob and Rezlescu, 1997; Kramer et al., 1990; Lawson and Gerber, 1990; Luborsky and Drummond, 1976, 1975; Murariu et al., 1998; Parker, 1988; Prenger et al., 1993; Schake et al., 1994; Schewe et al., 1980; Sheerer et al., 1981; Stekly and Minervini, 1981; Takayasu et al., 1976; Watson, 1973, 1978a,b; Worl et al., 1997), with particular emphasis placed on the transverse and longitudinal configurations and also the so-called capture cross section (λ) (Avens, 1996; Avens et al., 1992; Cowen et al., 1976; Cummings et al., 1976; Friedlaender et al., 1981a; Gerber, 1994; Gerber and Lawson, 1989; Gerber and Birss, 1983; Gerber, 1980; Lawson and Gerber, 1990; Prenger et al., 1993; Schake et al., 1994; Sheerer et al., 1981; Watson, 1973, 1978a; Worl et al., 1997). The capture cross section represents the maximum perpendicular distance that a particle can be from the flow streamline that passes through the center of the wire and still be retained. This parameter depends on many factors, of which the most important are the magnetic properties of both the suspended solids and the matrix, the applied field, the superficial velocity and the physical properties of the liquid (that is, density and viscosity), and the sizes of both the suspended particles and the matrix wires. The capture cross section also changes as the wire becomes increasingly loaded with retained material, and eventually goes to zero at saturation (Akoto, 1977; Cowen and Friedlaender, 1977; Cowen et al., 1976; Gerber, 1994, 1980; Gerber and Lawson, 1989; Gerber and Birss, 1983; Lawson and Gerber, 1990; Watson, 1978b).

The traditional way of obtaining λ has been through the use of trajectory models (Gerber, 1994, 1980; Gerber and Birss, 1983; Luborsky and Drummond, 1976, 1975), which

Correspondence concerning this article should be addressed to J. A. Ritter.

consist of partial differential equations that dynamically simulate the motion of a single particle toward a single wire when subjected to different forces. Although trajectory models are able to handle any configuration between the magnetic field and fluid flow, most of the correlations derived from trajectory models only address two particular configurations: longitudinal (that is, when the magnetic field and fluid flow are perpendicular to the wire and both parallel to each other) and transverse (that is, the same as in the longitudinal configuration, but when the magnetic field and fluid flow are perpendicular to each other) (Cowen et al., 1976; Gerber, 1994, 1980; Gerber and Birss, 1983; Luborsky and Drummond, 1976, 1975; Watson, 1978a). The first correlation that was obtained from a trajectory model, and has since been used by certain authors (Gerber and Lawson, 1989; Lawson and Gerber, 1990; Luborsky and Drummond, 1976, 1975), was developed by Watson (1973) for the longitudinal configuration over a clean wire. This correlation is valid for low magnetic-field conditions; it is also valid for the transverse configuration, as is demonstrated later (Gerber, 1994; Gerber and Birss, 1983). Its main drawback, however, is that it overlooks the effect of the short-range term of the magnetic force (that is, the term associated with the parameter α, as shown later), which thereby restricts its applicability to Watson's specific experimental conditions. Adjustments to the model were later introduced by Cowen et al. (Cowen et al., 1976; Watson, 1978a) to account for this limitation, but only for the case where the wire and particles have the same radius.

The first correlations developed for a wider spectrum of conditions were obtained by Gerber and coworkers (Gerber and Birss, 1983; Gerber, 1994) from analytical approximations of trajectory models for both the transverse and longitudinal configurations. The main restriction of these correlations, however, is that they only apply rigorously to extreme values of the magnetic field (that is, only at low and high values), and therefore lack the continuity that is needed in a single correlation. This problem is resolved here based on a new, single correlation that can be used to predict λ at all values of the magnetic field over a wide range of HGMS process conditions and for each configuration (that is, for both the longitudinal and transverse configurations). The basis behind this correlation and its development are described and discussed.

Trajectory Model

The trajectory model (Watson, 1973; Cummings et al., 1976; Friedlaender et al., 1981a; Gerber, 1994, 1980; Gerber and Birss, 1983; Kramer et al., 1990) used here assumes that a particle is moving in potential flow toward a single and clean wire of cylindrical shape, with its axis placed perpendicular to the direction of flow and with the magnetic field directed toward the two given directions, as shown in Figure 1. Several forces are relevant in the retention of a particle by a wire, among which the most important are the inertial, magnetic, viscous, gravitational, and Brownian forces. However, in liquid phase systems, where viscous effects are significant, inertial forces are normally assumed unimportant (Watson, 1973; Cummings et al., 1976; Friedlaender et al., 1981a; Gerber, 1994, 1980; Gerber and Birss, 1983; Kramer et al., 1990). Also, the particles are assumed large enough to neglect the disruptive effects of Brownian forces. Gerber and coworkers (Gerber, 1984; Gerber et al., 1983; Takayasu et al., 1976) have shown, for example, that depending on the magnetic susceptibility, the particle radii for which Brownian motion becomes important vary from 100 ($Mn_2P_2O_7$) to 700 nm (Al_2O_3) if stainless-steel wires of 100 μm diameter and fields of 8×10^5 A m^{-1} (that is, $B_o \approx 1$ T) are used. With these studies in mind, the following dimensionless differential force balance on a single particle in cylindrical coordinates is obtained (Cummings et al., 1976):

$$\begin{aligned} U_p' &= \frac{dr'}{d\tau} i_r + r' \frac{d\theta}{d\tau} i_\theta \\ &= U_f' - \frac{U_m}{U_o} \left\{ \left[\alpha \frac{1}{r'^5} \pm \cos(2\theta) \frac{1}{r'^3} \right] i_r \pm \right. \\ &\quad \left. \sin(2\theta) \frac{1}{r'^3} i_\theta \right\} - N_g [\cos(\theta) i_r - \sin(\theta) i] \end{aligned} \quad (1)$$

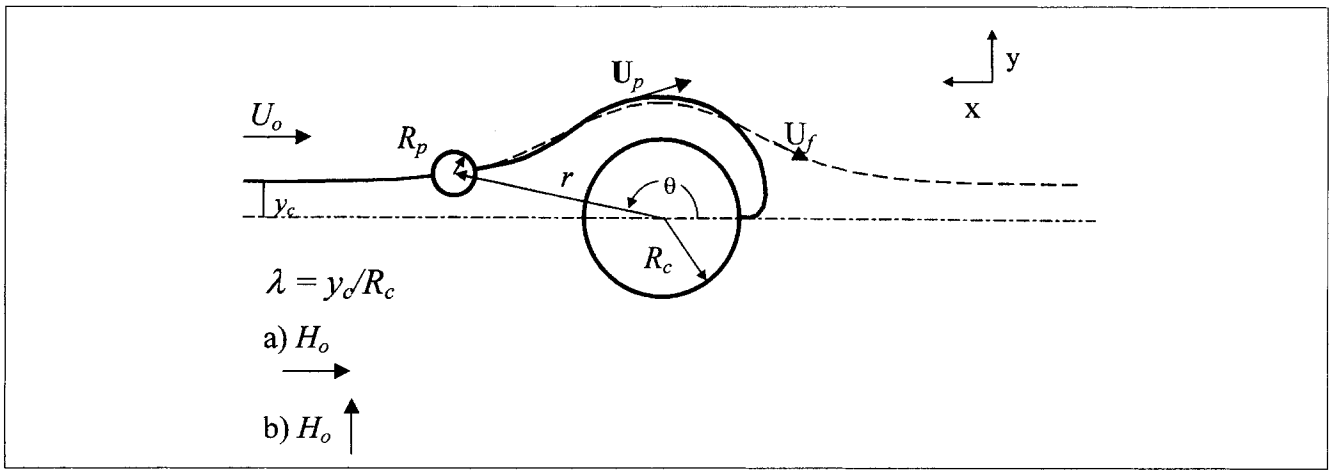

Figure 1. Side view of a particle of radius R_p approaching a matrix wire in a magnetic field H_o directed (a) parallel or (b) perpendicular to the flow with superficial velocity U_o and capture cross section y_c.

with

$$U_f' = \cos(\theta)\left(1 - \frac{1}{r'^2}\right) i_r - \sin(\theta)\left(1 + \frac{1}{r'^2}\right) i_\theta \tag{2}$$

$$\frac{U_m}{U_o} = \frac{2\alpha}{3} \frac{Re_c N_m \Gamma}{s^2} \tag{3}$$

$$\alpha = \frac{M_c}{2H_o} = \frac{\mu_c - \mu_o}{\mu_c + \mu_o} \tag{4}$$

$$\Gamma = \frac{\mu_p - \mu_o}{\mu_p + 2\mu_o} \tag{5}$$

$$N_m = \frac{\mu_o H_o^2}{\rho_f U_o^2} \tag{6}$$

$$s = \frac{R_c}{R_p} \tag{7}$$

$$Re_c = \frac{2\rho_f U_o R_c}{\eta_f} \tag{8}$$

$$N_g = \frac{2R_p^2(\rho_p - \rho_f)g}{9\eta_f U_o} \tag{9}$$

$$r' = \frac{r}{R_c}, \qquad \tau = \frac{tU_o}{R_c}, \qquad U_f' = \frac{U_f}{U_o}, \qquad U_p' = \frac{U_p}{U_o}, \tag{10}$$

where ρ_f and ρ_p are the densities of the fluid and particles, respectively; η_f is the viscosity of the fluid; μ_o, μ_c, and μ_p are the volumetric susceptibilities of vacuum (which is close to that of the fluid), the wire, and the particle, respectively; R_p is the radius of the particle; M_c and H_o are the magnetization of the matrix fiber and applied field, respectively; U_m is the so-called magnetic velocity, and U_p and U_f are the vectorial velocities of the particle and liquid, respectively, with the latter under potential flow and interstitial velocity U_o. Note that the preceding equations are slightly different from those in the work of Cummings (1976), where the chosen characteristic length was the radius of the particle R_p; here it is the radius of the wire R_c. In terms of these variables, a dimensionless capture cross section is defined as

$$\lambda = \frac{y_c}{R_c} \tag{11}$$

and is shown in Figure 1. The plus and minus signs in Eq. 1 stand for the fluid flow and magnetic field being parallel (longitudinal) and perpendicular (transverse), respectively. It is also important to remark that the values of λ obtained from Eq. 1 are valid only for the early stages of retention dynamics on the wire because the trajectory model is based on a clean matrix wire. Although the effect of a loaded matrix wire on λ is very important (Akoto, 1977; Cowen and Friedlaender, 1977; Cowen et al., 1976; Gerber, 1994, 1980; Gerber and Lawson, 1989; Gerber and Birss, 1983; Lawson and Gerber, 1990; Watson, 1978b), it is beyond the scope of this study.

Three independent dimensionless groups can be identified in Eq. 1. These are α, which appears in the short-range term of the radial component of the magnetic force in Eq. 1, N_g, which is next to the gravitational term, and the ratio U_m/U_o that appears on the lefthand side of the magnetic force. The parameter α is the demagnetizing factor and represents the fraction of the field that is reduced from H_o when it goes through a material with a magnetic permeability that is different from that of the medium and with magnetic poles in the direction of the applied field (see Eq. A8 in the Appendix). In paramagnetic materials, α is always less than unity and independent of the field H_o (since for paramagnetic materials M_c is linearly dependent on the applied field H_o). In ferromagnetic materials, such as stainless steel, however, it can be shown (see the Appendix, Eq. A12 and Watson, 1978) that α can attain values larger than unity, especially if the applied field is smaller than one-half the remanence magnetization and close in magnitude to the coercive force of the material (that is, stainless steel). In this situation it happens that the net internal field on the wire, that is, the sum of the applied and demagnetization fields, points against the applied field H_o (see Eq. A7). However, ferromagnetic materials made of annealed ferritic stainless steel are extremely soft and present coercive fields lower than 1000 A m^{-1} (Chen, 1986), and thus, at very low applied fields H_o (say 20,000 A m^{-1}, or $B_o \approx 0.025$ T) α rapidly approaches unity from a value that is initially greater than unity and stays there approximately until reaching saturation of the matrix (that is, when $H_o \approx M_{c,s}/2$), then it starts to decrease (Cowen et al., 1976; Friedlaender et al., 1978; Takayasu et al., 1983). This is why in most practical situations of HGMS, α can be assumed to be between 0 and 1. The parameter α can also be viewed as the ratio of the short-range magnetic force (that is, the fifth-order term in Eq. 1) to the long-range magnetic force (that is, the third-order term in Eq. 1), and because of this it usually has no role under very strong magnetic conditions (Gerber, 1994, 1980; Gerber and Birss, 1983). The terms U_m/U_o and N_g, on the other hand, represent ratios of the long-range magnetic and gravitational forces, respectively, to the fluid drag force. The effect of gravity, although small and normally ignored (Avens, 1996; Avens et al., 1992; Cummings et al., 1976; Friedlaender et al., 1981a,b; Gerber et al., 1996; Gerber, 1994, 1980; Gerber and Lawson, 1989; Gerber and Birss, 1983; Kramer et al., 1990; Lawson and Gerber, 1990; Luborsky and Drummond, 1976, 1975; Prenger et al., 1993; Schake et al., 1994; Watson, 1973, 1978; Worl et al., 1997), is examined here to make the correlation more complete.

Similar to Watson (1973) and others (Cowen et al., 1976), the trajectory model, depicted in Eqs. 1 to 10, is used here to generate values of the capture cross section for a wide range of conditions and properties by varying α and U_m/U_o. Since U_m/U_o and α appear to be related through Eq. 3, U_m/U_o can alternatively be split into two dimensionless groups by rewritting Eq. 3 as

$$\frac{U_m}{U_o} = \frac{2}{3}\alpha\beta, \tag{12}$$

with β being simply

$$\beta = \frac{Re_c N_m \Gamma}{S^2}. \tag{13}$$

In this way, it is straightforward to observe how the capture cross section varies with respect to α and β. Although β has no clear physical meaning, its selection as an alternative dimensionless group to U_m/U_o is shown later to be mathematically essential in obtaining a single correlation for the capture cross section.

The trajectory model was run for several values of α and β while keeping the dimensionless capture cross section lower than ten. The effect of gravity was also investigated by keeping $N_g = 0.0$ or 0.2. Moreover, to obtain an accurate correlation, the parameters α and β were varied over very wide ranges of values; however, it is important to emphasize that for the particular case of α, only values less than or equal to unity have practical meaning. With this in mind, the following ranges for parameters α and β were chosen

$$0.0002 \le \alpha \le 10{,}000 \tag{14}$$

$$0.0001 \le \beta \le 10{,}000. \tag{15}$$

To assure sufficient accuracy, a fourth-order Runge-Kutta method was utilized to obtain the solution to Eqs. 1 to 10 in terms of r' and θ, that is, the trajectory of the particle around the wire (see Figure 1). All of the simulations were initiated by setting the initial condition equal to ten fiber radii away from the fiber in the x-direction (see Figure 1) to start the trajectory of the particle from a position where it is only moved by the fluid flow. Then, for a given α and β and starting essentially at $y = 0$, increasingly larger values of y were selected until the particle just escaped the magnetic force field and was not retained by the wire. The previous value of y that caused the particle to be captured was denoted as the capture cross section for the selected values of α and β, or, $y_c = f(\alpha,\ \beta = 3U_m/2U_o\alpha)$. It is noteworthy, however, that different from other trajectory models, it was also assumed that the surface was perfectly smooth, meaning that once the particle hit the surface, it moved freely along the surface in the direction of the net tangential force. However, if the particle felt a repulsive force in the normal direction before reaching an equilibrium position, it left the surface and returned back to the flow. This procedure was repeated for the two different field orientations (that is, transverse and longitudinal) shown in Figure 1. After collecting sufficient data, correlations between λ, and α and β for both situations were developed. The results are given below.

Results and Discussion

Figure 2a shows the results obtained from the dynamic runs with the trajectory model for both magnetic-field configurations and for different values of α and β. Some of the data points in Figure 2a were recast in terms of the traditional parameters α and U_m/U_o; these results are shown in Figure 2b. The lines and arrows in both figures are included only to guide the eyes and to differentiate between the points with similar values of β or U_m/U_o. There are several interesting points to mention about the results in Figure 2. First, slightly larger values are obtained for the case when the magnetic field is perpendicular to the fluid flow (solid circles) compared to when it is parallel (open triangles), especially at large values of λ. This is merely due to the difference between the

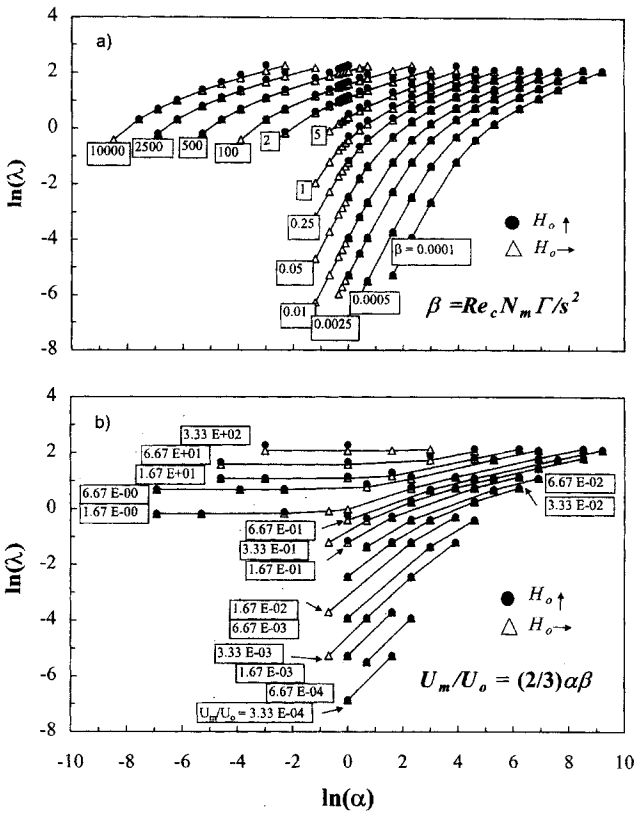

Figure 2. Capture cross sections (λ) obtained from the trajectory model for a wide range of α and β values and for the two magnetic-field orientations.

distributions of the magnetic field in both configurations. When the field is perpendicular to the flow, the attractive poles of the matrix wire are at $\theta = 90$ and 270°, and when the field is parallel to the flow the attractive poles are at $\theta = 0$ and 180°. In the latter case, the particles must be closer to the matrix to be retained under the same conditions. This result alone, however, does not indicate that the perpendicular configuration is better than the parallel one because the performance also depends on the saturation loading of the matrix, which is not treated here. The void space observed for values of $\alpha < 0.14$ (that is, $\ln \alpha \approx -2.0$) and $\lambda < 0.4$ (that is, $\ln \lambda \approx -1.0$) is another interesting feature. It is caused by the smooth-surface assumption, and therefore, the particles in this region are driven away by the flow because the viscous drag on the particle overwhelms both the short-ranged (that is, small α) and long-ranged (that is, small U_m/U_o) magnetic forces. This result also indicates that HGMS processes operated under these conditions would be very inefficient and should be avoided.

It is also interesting that when λ is expressed as a function of α and U_m/U_o, as in Figure 2b, it becomes independent of α (that is, $\alpha < 1$) for high and constant values of U_m/U_o. In particular, this is true when $U_m/U_o > \sqrt{2}$, which is in agreement with that reported elsewhere (Gerber, 1994; Gerber and Birss, 1983). This happens when the ratio of the long-ranged magnetic force to the drag force is large (that is, U_m/U_o), and

hence the role of the short ranged-force (that is, α) in the entrapment of a paramagnetic particle approaching from a critical distance is small or negligible. Under these conditions, the paramagnetic particle is irreversibly trapped far from the surface of the wire (that is, large λ).

The most interesting characteristic observed in Figure 2a, however, is that all of the curves amazingly appear to be quite similar when λ is represented in terms of α and β. This is not at all true when λ is plotted as a function of α and U_m/U_o. Thus, as stated earlier and as shown below, the idea of choosing α and β in lieu of α and U_m/U_o as the independent parameters turned out to be instrumental in obtaining a single correlation for the whole spectrum of variables and conditions governing HGMS. First, it was speculated that the similar appearance of all of the curves in Figure 2a inferred that their shape was independent of β. Moreover, all of them exhibited two different and clearly distinguishable linear regions with a smooth transition occurring at around $\lambda \approx 0.6$. They were also systematically displaced from one another in the direction of the $\ln\alpha$ axis, indicating that the distances (that is, in the direction of the α-axis) between any curves having fixed values of β were independent of λ. The preceding parallelism indicated that if a reference value $\ln\lambda_o$ was selected and the corresponding values of α denoted as α_o were determined for each of the curves in Figure 2a, then for each of these curves, any value of $\ln\alpha$ relative to $\ln\alpha_o$ (that is, $\ln\alpha - \ln\alpha_o$) would produce identical values of λ. This observation suggested that all of the curves in Figure 2a would collapse into a single curve by expressing $\ln\lambda$ in terms of $\ln\alpha - \ln\alpha_o$. Moreover, if a relationship between β and α_o could be found, a much simpler relationship between λ, and the parameters α and β, would be obtained. This relationship was obtained by plotting $\ln\alpha_o$ as a function of $\ln\beta$, with $\ln\lambda_o$ arbitrarily set to zero, as shown in Figure 3.

Figure 3 reveals two clearly distinguishable linear zones with a sharp transition occurring at around $\beta = 5$. As a consequence, four clearly defined regions could be realized (that is, two defined by $\ln\beta$ times the two already observed in Figure 2a) in the relationship between $\ln\lambda$ and the dimensionless groups $\ln\beta$ and $\ln\alpha$. This unique result suggested the following correlation of combinations of linear functions (denoted in brackets) between $\ln\alpha_o$ and $\ln\beta$, and $\ln\lambda$ and $(\ln\alpha - \ln\alpha_o)$

$$c_1 = [\ln\alpha_o - a_1\ln\beta - b_1][\ln\alpha_o - a_2\ln\beta - b_2] \quad (16)$$

$$c_2 = [\ln\lambda - d_1(\ln\alpha - \ln\alpha_o) - e_1][\ln\lambda - d_2(\ln\alpha - \ln\alpha_o) - e_2]. \quad (17)$$

Equations 16 and 17 represent a set of two hyperbolic functions with asymptotes as the linear trends observed in Figures 2a and 3, and the transition smoothness defined by the values of c_1 and c_2. These two equations can be expressed explicitly in terms of $\ln\alpha_o$ and $\ln\lambda$ according to

$$\ln\alpha_o = \frac{-A_o - \sqrt{A_o^2 - 4C_o}}{2} \quad (18)$$

$$\ln\lambda = \frac{-A - \sqrt{A^2 - 4C}}{2}, \quad (19)$$

where

$$A_o = -[(a_1 + a_2)\ln\beta + (b_1 + b_2)] \quad (20)$$

$$C_o = (a_1\ln\beta + b_1)(a_2\ln\beta + b_2) \quad (21)$$

$$A = -[(d_1 + d_2)(\ln\alpha - \ln\alpha_o) + (e_1 + e_2)] \quad (22)$$

$$C = [d_1(\ln\alpha - \ln\alpha_o) + e_2][d_2(\ln\alpha - \ln\alpha_o) + e_2]. \quad (23)$$

The minus sign to the left of the square-root expression in both Eqs. 18 and 19 ensures the correct convexity of the curves in Figures 2a and 3. These two equations contain ten adjustable parameters (that is, a_1, a_2, b_1, b_2, c_1, c_2, d_1, d_2, e_1, and e_2) that were obtained by fitting this correlation to the capture cross section values obtained from the trajectory model. However, four of them (that is, a_1, a_2, d_1, and d_2) were already defined (approximately) by the slopes of the linear zones of the curves in Figures 2a and 3. These values were therefore used as good initial guesses in a nonlinear regression routine. The resulting correlation parameters are shown in Table 1 for both orientations of the magnetic field.

Figure 4 compares the values of λ obtained from the trajectory model to those obtained from the correlation for both flow and field configurations. Some deviations were observed in both situations at values of λ larger than four, and especially for the case when the field and flow were in the same direction. In this case, a maximum error of 17.7% was observed, but with an overall average error of only 4.2%. Better results were obtained, however, for the case when the field was perpendicular to the flow, with maximum and average errors of only 10.3 and 2.6%, respectively. These slight deviations suggested that the shapes of the curves were not totally independent of the value of β, especially at large applied fields (which was consistent with large values of λ). They were caused by the fact that at such large fields the initial x-direction condition of the trajectory model was not far enough from the fiber to be free from its magnetic influence and therefore at such a position the particle could no longer move parallel to the x-direction. Despite the preceding, Figure 5

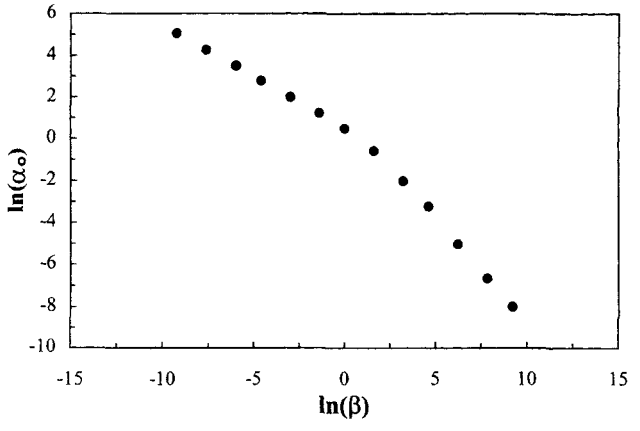

Figure 3. Dependency between the relative positions of the curves in Figure 2 in terms of $\ln\alpha_o$ as a function of $\ln\beta$ for an arbitrary reference plane, $\ln\lambda = 0.0$.

Table 1. Parameters for the New Capture Cross-Section Correlation (Eqs. 16 and 17) with Magnetic Field and Flow Parallel (Longitudinal) and Perpendicular (Transverse)

Parameter	Magnetic Field ∥ to Flow	Magnetic Field ⊥ to Flow
a_1	−0.49480	−0.48990
a_2	−1.00603	−1.02248
b_1	0.19565	0.52197
b_2	1.05324	1.50099
c_1	0.05207	0.36778
c_2	3.57310	1.66374
d_1	0.24419	0.34487
d_2	2.20249	2.07542
e_1	1.17855	0.77117
e_2	2.30095	2.07217
Max. error (%)*	17.7	10.3
Avg. error (%)**	4.2	2.6

*Error (%): $\epsilon = 100 \mid \lambda_{cal} - \lambda_{corr} \mid \lambda$ cal.
**Average error (%): $\bar{\epsilon} = (1/n) \sum_{i=1}^{n} \epsilon_i$.

shows that in both situations the correlation (solid lines) agreed very well with the behavior observed from the trajectory model (symbols).

The effect of gravity was also investigated at a relatively high value of N_g. Figure 5 shows the results for the particular

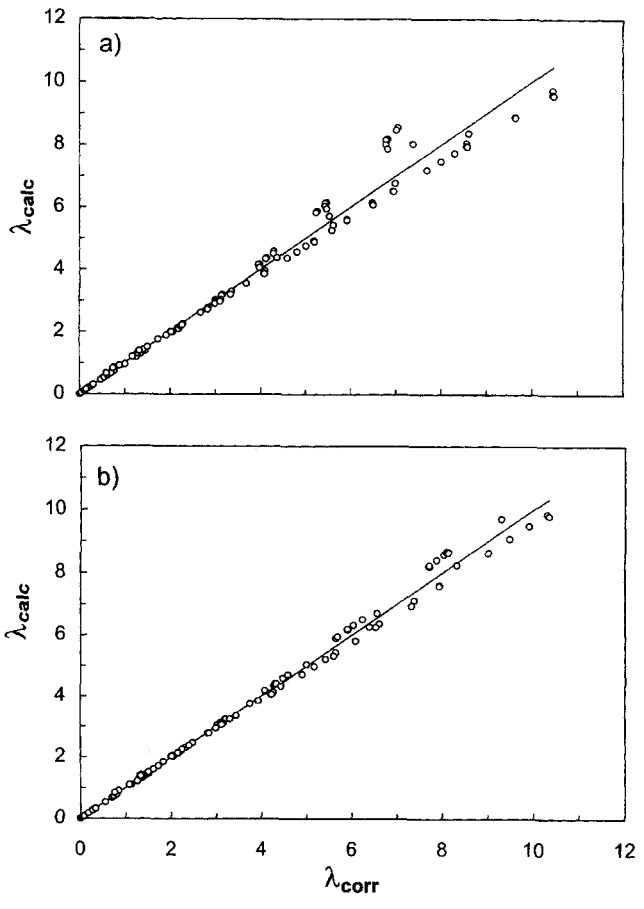

Figure 4. Capture cross sections from the trajectory model (λ_{calc}) vs. those from the new correlation (λ_{corr}) for the (a) longitudinal and (b) transverse cases in Table 1.

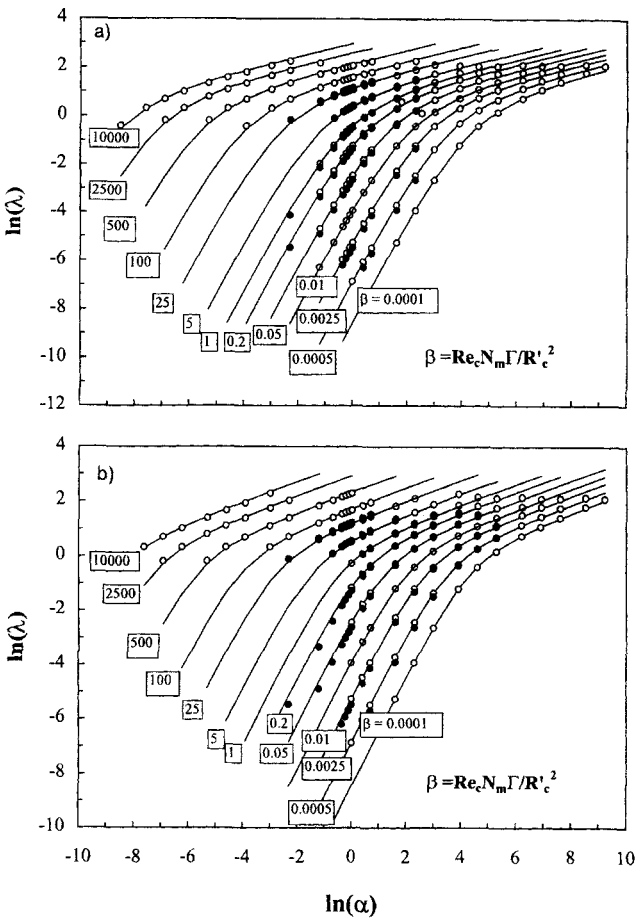

Figure 5. Capture cross sections (λ) obtained from the trajectory model with $N_g = 0.0$ (open circles) and $N_g = 0.2$ (solid circles) vs. those from the correlation with $N_g = 0.0$ (lines) for the (a) longitudinal and (b) transverse cases in Table 1.

case with $N_g = 0.2$. As expected, the results show that the trajectory model was relatively insensitive to the effect of gravity when N_g was less than about 0.2. In both situations the error was never larger than about 10%. This result was consistent with that reported elsewhere (Lawson and Gerber, 1990; Gerber and Lawson, 1989; Watson, 1973; Cummings et al., 1976; Worl et al., 1997; Avens, 1996; Schake et al., 1994; Prenger et al., 1993; Avens et al., 1992; Friedlaender et al., 1981 a,b; Luborsky and Drummond, 1976, 1975; Gerber et al., 1996; Kramer et al., 1990).

Figure 6 compares the results from the new correlation with those obtained by Watson (1973) from a similar trajectory model in terms of U_m/U_o. The agreement between his results and the ones predicted by the new correlation was quite satisfactory, with only minor differences observed in the region close to the origin. These differences were caused by the fact that the singular point obtained from the trajectory model (see Gerber and Birss, 1983) fell within the wire, so that smaller results were obtained from the "smooth surface" assumption utilized here as opposed to the "hit and stay" assumption utilized by Watson. It must be emphasized, how-

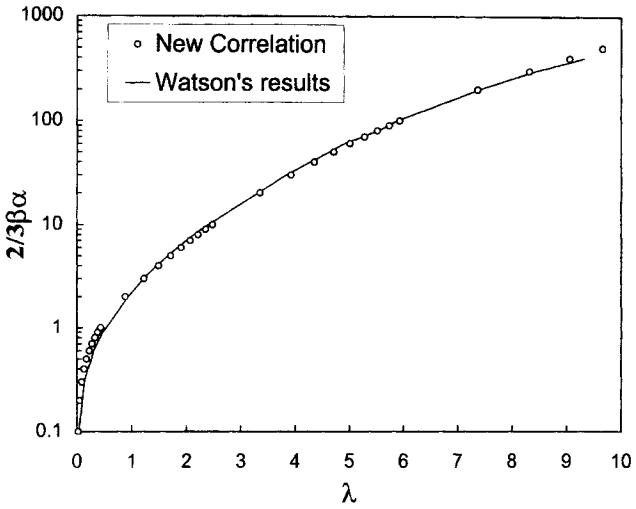

Figure 6. New correlation vs. trajectory results by Watson (1973) that apply only to $\alpha = 0.0669$.

ever, that Watson obtained his trajectory results for the particular case of $\alpha = 0.0669$; therefore, the correlation he derived from them was quite limited in its range of application. In contrast, the new correlation extends this range for any feasible and practical values of α, making it applicable to a wide range of HGMS conditions. The importance of this work becomes even more apparent by noting that Watson's correlation has been applied erroneously in the literature (Lawson and Gerber, 1990; Gerber and Lawson, 1989; Luborsky and Drummond, 1976, 1975) to situations where the value of α was not even close to 0.0669. This was especially serious when the applied field was such that $U_m/U_o < \sqrt{2}$, a condition where λ depends not only on U_m/U_o but also on α (Gerber, 1994; Gerber and Birss, 1983).

In this regard, Gerber et al. (Gerber, 1994; Gerber and Birss, 1983) presented the following analytical approximations for the two different field configurations. When $U_m/U_o < \sqrt{2}$,

$$\lambda = \frac{1}{2}\frac{U_m}{U_o}\left\{(1-\alpha^2)^{0.5} + \alpha[\pi - a\cos(\alpha)]\right\} \qquad (24)$$

for the longitudinal configuration, and

$$\lambda = \frac{1}{2}\frac{U_m}{U_o}\left\{(1-\alpha^2)^{0.5} + \alpha[2\pi - a\cos(\alpha)]\right\} \qquad (25)$$

for the transverse configuration. When $U_m/U_o > \sqrt{2}$,

$$\lambda = \frac{3}{4}\sqrt{3}\left(\frac{U_m}{U_o}\right)^{1/3}\left[1 - \frac{2}{3}\left(\frac{U_m}{U_o}\right)^{-2/3}\right] \qquad (26)$$

for both configurations. These approximations are compared to the new correlation for practical ranges of α and U_m/U_o in Figures 7 and 8 for the longitudinal and transverse configurations, respectively. In general, the agreement was not very good at low field conditions (that is, $U_m/U_o < \sqrt{2}$), especially

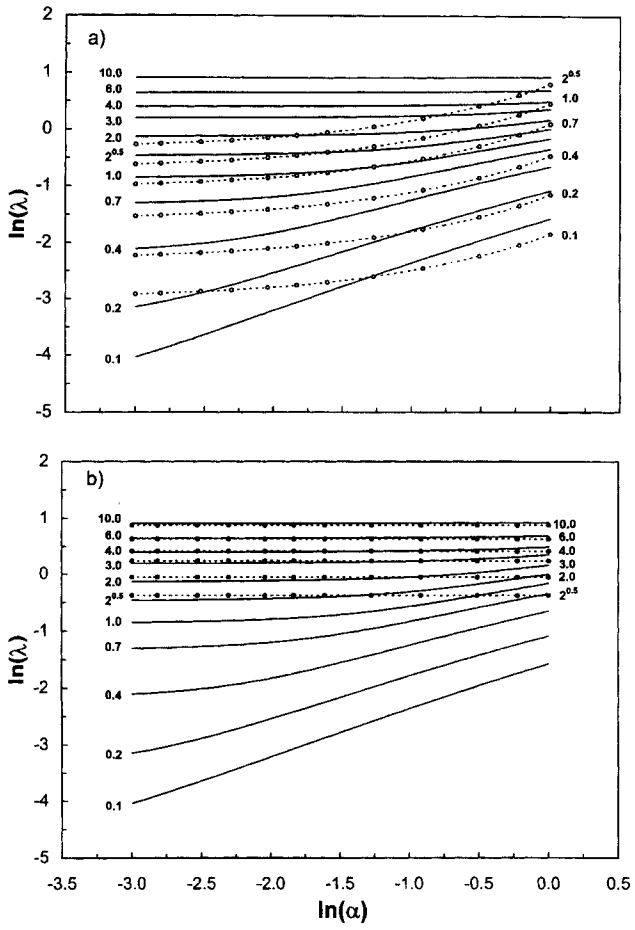

Figure 7. New correlation (solid lines) vs. correlation by Gerber et al. (Gerber, 1994; Gerber and Birss, 1983) for the longitudinal configuration with (a) $U_m/U_o < \sqrt{2}$ (○ . . .) and (b) $U_m/U_o > \sqrt{2}$ (● . . .).

close to the transition zone (that is, $U_m/U_o = \sqrt{2}$). Again, as with Watson's results, the lower values of λ observed for the new correlation were mainly due to the smooth surface assumption utilized in this work. However, the differences observed at higher values of α, and especially close to the transition zone (that is, intermediate values of U_m/U_o), were mainly due to the approximations utilized by Gerber and Birss (1983) to derive Eqs. 24 and 25. In this case, the singular points of the trajectory model fell outside the wire, and therefore the assumptions involved in Eqs. 24 and 25 were no longer valid. Different results were obtained, however, for high field conditions (that is, $U_m/U_o > \sqrt{2}$), where satisfactory agreement was observed with these approximate models and the new correlation, especially at low values of α. The new correlation also reveals that λ becomes independent of α for large values of U_m/U_o; this trend is not observed with the approximate models. Overall, the main advantage of the new correlation over the approximate analytical models developed by Gerber et al. (Gerber, 1994; Gerber and Birss, 1983) is its ability to cover the entire spectrum of practical fields (that is, U_m/U_o values) with very good accuracy, as shown in Figure 4.

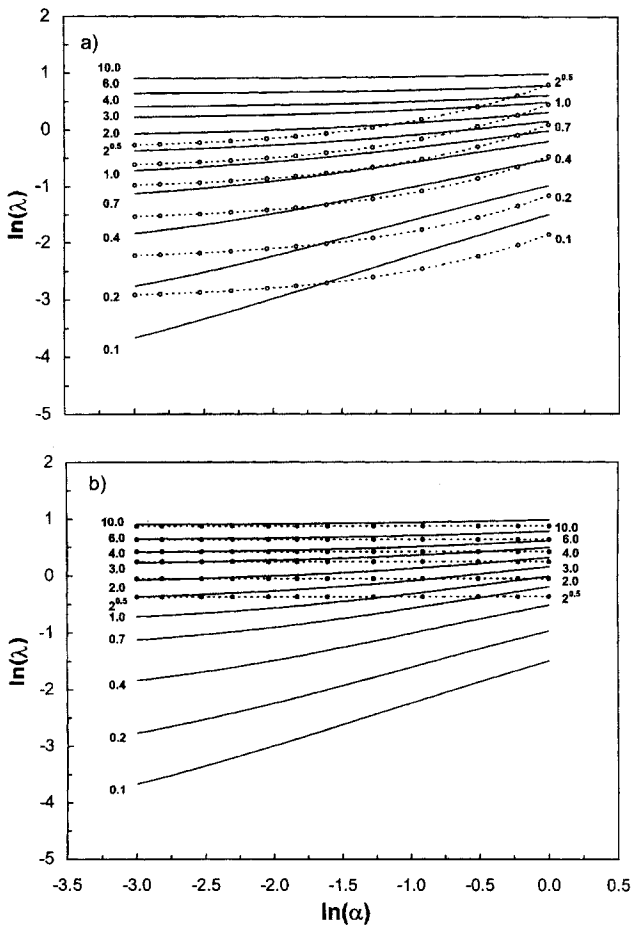

Figure 8. New correlation (solid lines) vs. correlation by Gerber et al. (Gerber, 1994; Gerber and Birss, 1983) for the transverse configuration with (a) $U_m/U_o < \sqrt{2}$ (○ . . .) and (b) $U_m/U_o > \sqrt{2}$ (● . . .).

The only issue that remains to be addressed is how to apply this correlation to an actual HGMS process. The operation of an HGMS process is governed by the two dimensionless groups α and β. Thus, for a given set of process conditions, and the appropriate set of correlation parameters from Table 1, λ is determined as follows: for a particular value of β, A_o, and C_o are calculated from Eqs. 20 and 21, respectively, and then these values are used to calculate α_o from Eq. 18. For the particular value of α, and using the α_o just obtained, A and C are calculated from Eqs. 22 and 23, respectively, and then these values are used to calculate λ from Eq. 19. It is important to stress that β does not need to appear in the preceding relations; the same can be done by using only α and U_m/U_o if the relationship between β and these two variables (that is, Eq. 12) is directly inserted into the previous relationships (that is, Eqs. 18 to 23). Clearly, with this explicit solution methodology, this correlation can be easily incorporated into a fixed-bed HGMS-process model to describe the retention dynamics of suspensions. It should also be easy to account for polydispersities in both particle size and particle magnetic susceptibility by applying the appropriate distribution functions along with these correlations in a fixed-bed HGMS model.

Conclusions

A new, relatively easy to use and very robust correlation was developed for the determination of the capture cross section (λ) in HGMS systems. This correlation covers much broader ranges of process conditions and physical properties compared to the current correlations and approximate analytical models in the literature. Thus, it should prove to be very useful in the design, development, optimization, and modeling of HGMS processes.

This new correlation was formulated in terms of combinations of linear functions based on four linear regions observed in the log-log domain between λ and the dimensionless groups α and β. These linear trends were quite remarkable and the reason why the correlation adequately predicted the behavior of the trajectory model over such broad spectrums of α and β. Results not shown in this work indicated that these linear trends persisted even if the "hit and stay" assumption was applied, and even if the initial conditions for the trajectory model were changed such that the particle started at a distance greater than ten radii from the fiber, as used in this work. Thus, the formulation behind the correlation is recommended not only for its simplicity but also for its robustness through a variety of assumptions.

This work, however, only considered the situation where the wire was completely clean, and therefore, the correlations are rigorously applicable only for the early stages of retention dynamics. Loading effects on λ are of paramount importance because, as the wire becomes increasingly loaded, the new incoming particles cannot get as close to the ferromagnetic element, which may reduce the values of λ considerably. Future work should address this issue.

Finally, the main utility of this correlation is its application in modeling HGMS processes that involve solutions containing suspensions of particles that are polydisperse in both size and magnetic susceptibility. Because of the complexity of this situation, models available in the literature that have attempted to predict or correlate the behavior of an HGMS system, have assumed the solution to be composed of particles of the same size and magnetic susceptibility. However, this new correlation greatly facilitates the modeling of heterogeneous systems, because it is straightforward to relate λ to the preceding two variables. Future work should use these correlations to compare the accuracy of the single size–single magnetic susceptibility models in predicting the more complex and realistic situations associated with polydispersity.

Acknowledgments

The authors gratefully acknowledge financial support from the National Science Foundation under Grant CTS-9985489. The authors also acknowledge the insightful comments about this work from Professor Richard Gerber at the University of Salford, England.

Notation

A = parameter in Eq. 22
A_o = parameter in Eq. 20
a = coefficient of the magnetic potential within the wire defined in Eq. A3a, $A \cdot m^{-1}$

a_1 = adjustable parameter in Eq. 16
a_2 = adjustable parameter in Eq. 16
b = coefficient of the magnetic potential external to the wire defined in Eq. A3b, A·m
b_1 = adjustable parameter in Eq. 16
b_2 = adjustable parameter in Eq. 16
B_o = magnetic induction of the applied field, T
$B_{i,\text{total}}$ = total magnetic induction within the wire, T
C = parameter in Eq. 23
C_o = parameter in Eq. 21
c_1 = adjustable parameter in Eq. 16
c_2 = adjustable parameter in Eq. 17
d_1 = adjustable parameter in Eq. 17
d_2 = adjustable parameter in Eq. 17
e_1 = adjustable parameter in Eq. 17
e_2 = adjustable parameter in Eq. 17
g = gravitational constant, $m \cdot s^{-2}$
H_c = coercive force field of the wire, $A \cdot m^{-1}$
H_d = demagnetization field of the wire, $A \cdot m^{-1}$
$H_{e,\text{total},r}$ = radial component of the total magnetic field outside the wire, $A \cdot m^{-1}$
$H_{i,\text{total}}$ = total magnetic field within the wire, $A \cdot m^{-1}$
$H_{i,\text{total},r}$ = radial component of the total magnetic field within the wire, $A \cdot m^{-1}$
H_o = external applied field, $A \cdot m^{-1}$
i_θ = θ vectorial component in cylindrical coordinates
i_r = r vectorial component in cylindrical coordinates
k = linear slope of the dependence of M_c on $H_{i,\text{total}}$, Eq. A1
M_c = magnetization of the wire, $A \cdot m^{-1}$
$M_{c,r}$ = remanence magnetization of the wire, $A \cdot m^{-1}$
$M_{c,s}$ = magnetization of the wire at saturation, $A \cdot m^{-1}$
N_g = dimensionless number, ratio between gravity and viscous forces, Eq. 9
N_m = dimensionless number, ratio between magnetic and kinetic energies, Eq. 6
r = distance from the center of the wire to the center of the particle, m
r' = dimensionless r relative to R_c, Eq. 10
R_c = radius of the wire, m
R_p = radius of the particle, m
Re_c = Reynolds number of the liquid phase, Eq. 8
s = ratio of R_c to R_p, Eq. 6
t = time, s
U_o = interstitial velocity of the liquid phase, $m \cdot s^{-1}$
$\boldsymbol{U}_f$ = vectorial velocity of the fluid under potential flow, $m \cdot s^{-1}$
$\boldsymbol{U}_p$ = vectorial velocity of the particle, $m \cdot s^{-1}$
$\boldsymbol{U}'_f$ = dimensionless ratio of $\boldsymbol{U}_f$ to U_o
U_m = magnetic velocity defined according to Eq. 3, $m \cdot s^{-1}$
$\boldsymbol{U}'_p$ = dimensionless ratio of $\boldsymbol{U}_p$ to U_o
y_c = capture cross section, m

Greek letters

α = demagnetizing factor for a wire
α_o = demagnetizing factor for an arbitrary ln λ
β = dimensionless group defined according to Eq. 13
ϕ_i = magnetic potential within the wire defined according Eq. A3a, A
ϕ_e = magnetic potential outside the wire defined according Eq. A3b, A
Γ = demagnetization factor for a sphere and defined in Eq. 5
η_f = viscosity of the liquid phase, Pa·s
λ = dimensionless ratio of y_c to R_c
μ_f = magnetic permeability of the liquid phase, $T \cdot m \cdot A^{-1}$
μ_p = magnetic permeability of the particle, $T \cdot m \cdot A^{-1}$
θ = angle defined according to Figure 1
ρ_f = density of the liquid phase, $kg \cdot m^{-3}$
ρ_p = density of the particle, $kg \cdot m^{-3}$
τ = dimensionless ratio of t to R_p/U_o, Eq. 10

Subscripts

calc = from the trajectory model
corr = from the correlation model

Literature Cited

Akoto, I. Y., "Mathematical Modeling of High-Gradient Magnetic Separation Devices," *IEEE Trans. Magn.*, **MAG-13**, 1486 (1977).

Avens, L. R., "Use of High Gradient Magnetic Separation for Actinide Applications," U.S. DOE Rep. LANL LA-UR-96-2064 (1996).

Avens, L. R., L. A. Worl, K. J. de Aguero, F. C. Prenger, W. F. Stewart, D. D. Hill, and T. L. Tolt, "Environmental Remediation Using Magnetic Separation," AIChE Meeting, Miami Beach, FL (1992).

Birss, R. R., R. Gerber, M. R. Parker, and T. J. Sheerer, "Laminar Flow Model of Particle Capture of Axial Magnetic Filters," *IEEE Trans. Magn.*, **MAG-14**, 1165 (1978).

Birss, R. R., R. Gerber, and M. R. Parker, "Theory and Design of Axially Ordered Filters for High Intensity Magnetic Separation," *IEEE Trans. Magn.*, **MAG-12**, 892 (1976).

Chen, C.-W., *Magnetism and Metallurgy of Soft Magnetic Materials*, Dover, New York (1986).

Cowen, C., and F. J. Friedlaender, "Single Wire Model of High Gradient Magnetic Separation Processes III," *IEEE Trans. Magn.*, **MAG-13**, 1483 (1977).

Cowen, C., F. J. Friedlaender, and R. Jaluria, "Single Wire Model of High Gradient Magnetic Separation Processes I," *IEEE Trans. Magn.*, **MAG-12**, 466 (1976).

Cummings, D. L., D. A. Himmelblau, and J. A. Oberteuffer, "Capture of Small Paramagnetic Particles by Magnetic Forces from Low Speed Fluid Flows," *AIChE J.*, **22**, 569 (1976).

Friedlaender, F. J., R. Gerber, H.-P. Henkel, and R. R. Birss, "Particle Buildup on Single Spheres in HGMS," *IEEE Trans. Magn.*, **MAG-17**, 2801 (1981a).

Friedlaender, F. J., R. Gerber, W. Kurz, and R. R. Birss, "Particle Motion Near and Capture on Single Spheres in HGMS," *IEEE Trans. Magn.*, **MAG-17**, 2804 (1981b).

Friedlaender, F. J., M. Takayasu, J. B. Rettig, and C. P. Kentzer, "Studies of Single Wire Parallel Stream Type HGMS," *IEEE Trans. Magn.*, **MAG-14**, 404 (1978).

Gerber, R., P. Krist, and L. Tarrant, "The Retention of Strongly Magnetic Particles in Single Wire HGMS," *IEEE Trans. Magn.*, **MAG-32**, 5100 (1996).

Gerber, R., "Magnetic Separation," *Applied Magnetism*, R. Gerber, C. D. Wright, and G. Asti, eds., Kluwer, Dordrecht, The Netherlands (1994).

Gerber, R., and P. Lawson, "The HGMS Filter Performance Exponential Law," *IEEE Trans. Magn.*, **MAG-25**, 3806 (1989).

Gerber, R., "Magnetic Filtration of Ultra-Fine Particles," *IEEE Trans. Magn.*, **MAG-20**, 1159 (1984).

Gerber, R., M. Takayasu, and F. J. Friedlaender, "Generalization of HGMS Theory: The Capture of Ultra-Fine Particles," *IEEE Trans. Magn.*, **MAG-19**, 2115 (1983).

Gerber, R., and R. R. Birss, *High Gradient Magnetic Separation*, Wiley, Chichester, UK (1983).

Gerber, R., "Particle Capture in High Gradient Magnetic Separation," *Physics Programs*, A. D. Boardman, ed., Wiley, Chichester, UK (1980).

Iacob, G., and N. V. Rezlescu, "Possibility of High Gradient Magnetic Separation in Angular Steps," *IEEE Trans. Magn.*, **MAG-33**, 4445 (1997).

Kramer, A. J., J. J. M. Janssen, and J. A. A. J. Perenboom, "Single-Wire HGMS of Colloidal Particles: The Evolution of Concentration Profiles," *IEEE Trans. Magn.*, **MAG-26**, 2801 (1990).

Lawson, P., and R. Gerber, "Viscosity Effects in Multi-Wire HGMS," *IEEE Trans. Magn.*, **MAG-26**, 1861 (1990).

Luborsky, F. E., and B. J. Drummond, "Buildup of Particles on Fibers in a High Field-High Gradient Separator," *IEEE Trans. Magn.* **MAG-12**, 463 (1976).

Luborsky, F. E., and B. J. Drummond, "High Gradient Magnetic Separation: Theory versus Experiment," *IEEE Trans. Magn.*, **MAG-11**, 1697 (1975).

Murariu, V., N. Rezlescu, O. Rotariu, and V. Badescu, "Concentration Influences on Recovery in a High Gradient Magnetic Separation Axial Filter," *IEEE Trans. Magn.*, **MAG-34**, 695 (1998).

Parker, M. R., "Novel HGMF/HCFS Magnetic Filter Design," *IEEE Trans. Magn.*, **MAG-24**, 2431 (1988).

Prenger, F. C., W. F. Stewart, D. D. Hill, L. R. Avens, A. R. Schake,

K. J. de Aguero, D. D. Padilla, L. A. Worl, and T. L. Tolt, "High Gradient Magnetic Separation Applied to Environmental Remediation," U.S. DOE Rep. LANL LA-UR-93-2516 (1993).
Schake, A. R., L. R. Avens, D. D. Hill, D. D. Padilla, F. C. Prenger, D. A. Romero, T. L. Tolt, and L. A. Worl, "Magnetic Separation for Environmental Remediation," U.S. DOE Rep. LANL LA-UR-94-3373 (1994).
Schewe, H., M. Takayasu, and F. J. Friedlaender, "Observation of Particle Trajectories in an HGMS Single-Wire System," *IEEE Trans. Magn.*, **MAG-16**, 149 (1980).
Sheerer, T. J., M. R. Parker, F. J. Friedlaender, and R. R. Birss, "Theory of Capture of Weakly Magnetic Particles in Random Matrices in the Longitudinal Configuration in HGMS," *IEEE Trans. Magn.*, **MAG-17**, 280 (1981).
Stekly, Z. J. J., and J. V. Minervini, "Shape Effect of the Matrix on the Capture Cross Section of Particles in High Gradient Magnetic Separation," *IEEE Trans. Magn.*, **MAG-12**, 474 (1976).
Takayasu, M., R. Gerber, and F. J. Friedlaender, "Magnetic Separation of Submicron Particles," *IEEE Trans. Magn.*, **MAG-19**, 2112 (1983).
Watson, J. H. P., "Improvements of a Low-Field, High-Intensity Matrix Separator," *IEEE Trans. Magn.*, **MAG-14**, 392 (1978a).
Watson, J. H. P., "Approximate Solutions of the Magnetic Separator Equations," *IEEE Trans. Magn.*, **MAG-14**, 240 (1978b).
Watson, J. H. P., "Magnetic Filtration," *J. Appl. Phys.*, **44**, 9, 4209 (1973).
Worl, L. A., D. D. Hill, D. D. Padilla, and F. C. Prenger, "High Gradient Magnetic Separation for Nuclear Material Collection," U.S. DOE Rep. LANL LA-UR-97-1508 (1997).

Appendix

At low total internal magnetic fields ($H_{i,\text{total}}$) and within the outermost hysteresis loop (that is, the magnetic path followed when turning off the applied field), the magnetization of a ferromagnetic cylinder can be assumed to follow a linear relationship with the total internal field according to

$$M_c = M_{c,r} + kH_{i,\text{total}}, \tag{A1}$$

where $M_{c,r}$ is the remanence magnetization of the wire material and k is of the order or approximately equal to

$$k = \left| \frac{M_{c,r}}{H_c} \right|, \tag{A2}$$

with H_c being the coercive field of the wire material. Under these circumstances, the divergenceless condition of the magnetic flux renders the following expressions in cylindrical coordinates for the scalar magnetic potential

$$\phi_i = -rH_o \cos\theta + ar\cos\theta \quad \text{if} \quad r \le R_c \tag{A3a}$$

$$\phi_e = -rH_o \cos\theta + \frac{b}{r}\cos\theta \quad \text{if} \quad r > R_c. \tag{A3b}$$

Also, the following two boundary conditions apply:

1. Continuity of the flux at the interface

$$\mu_o(H_{i,\text{total},r} + M_c \cos\theta) = \mu_o(H_{e,\text{total},r}); \tag{A4a}$$

2. Continuity of the scalar potential at the interface

$$\phi_i = \phi_e, \tag{A4b}$$

where the subscript r in the field terms indicates the radial component of the total field, with $H_{e,\text{total}}$ being the total external field. From Eqs. A1, A3, and A4, and knowing that

$$H_{i,\text{total},r} = -\frac{\partial \phi_i}{\partial r} \tag{A5a}$$

$$H_{e,\text{total},r} = -\frac{\partial \phi_e}{\partial r}, \tag{A5b}$$

it can be shown that

$$a = \frac{b}{R_c^2} = \frac{M_{c,r} + kH_o}{2+k}, \tag{A6}$$

and because all the field lines are parallel inside the cylindrical wire, the net value of the internal field is given by

$$H_{i,\text{total}} = -\frac{M_{c,r} + kH_o}{2+k} + H_o = \frac{2H_o - M_{c,r}}{2+k}, \tag{A7}$$

or, in terms of the demagnetizing factor α,

$$H_{i,\text{total}} = (1-\alpha)H_o, \tag{A8}$$

where α is given by

$$\alpha = \frac{M_{c,r}/H_o + k}{2+k}. \tag{A9}$$

The first term on the righthand side of Eq. A7 is the so-called demagnetization field of the cylindrical wire (normally referred to as H_d), which is generated by the formation of free magnetic poles at the surface when an applied field H_o is perpendicular to the axis of the cylindrical wire. These poles have opposing signs at each side of the wire, causing the field that is originated by them (that is, H_d) to point against the applied field (as indicated by the negative sign preceding the term). Notice from Eq. A7 that if $H_o < 1/2M_r$, the matrix is always under magnetization reversal, that is, the demagnetization field is strong enough for $H_{i,\text{total}}$ to oppose the applied field H_o (that is, negative). In most ferritic steels, $M_{c,r} > 400{,}000\ \text{A}\cdot\text{m}^{-1}$ (that is, $B_r \approx 0.5$ T) (Chen, 1986), which is quite a significant value and indicates that $H_{i,\text{total}}$ is positive only at relatively high applied fields. Also, notice that if k is very large, as in soft and annealed ferromagnetic materials, like ferritic stainless steels, the total internal field $H_{i,\text{total}}$ is very small (say less than $2{,}000\ \text{A}\cdot\text{m}^{-1}$).

Now, from Eqs. A1 and A7 the magnetization of the wire becomes

$$M_c = M_{c,r} + k\frac{2H_o - M_{c,r}}{2+k},$$

or

$$M_c = \frac{2}{2+k}M_{c,r} + \frac{2k}{2+k}H_o, \tag{A10}$$

which is also equal to, after substitution of Eq. A9,

$$M_c = 2\alpha H_o. \tag{A11}$$

Using Eq. A2 and assuming k large, Eqs. A10 and A11 finally show that

$$\alpha = \frac{M_c}{2H_o} \approx \frac{H_c}{H_o} + 1, \tag{A12}$$

which is identical to the expression obtained by Watson (Watson, 1978). It is clear from this last expression that as long as a linear dependence exists between the magnetization of the wire and the total internal field (that is, Eq. A1), α is larger than unity. In annealed ferritic stainless steel, however, H_c is normally very small (that is, $H_c < 1000\ \mathrm{A \cdot m^{-1}}$) (Chen, 1986), so it does not take much for the applied field to cause α to decrease rapidly to a value close to unity. Also, it is simple to show that from the constitutive equation of magnetic fields, that is,

$$B_{i,\mathrm{total}} = \mu_o(H_{i,\mathrm{total}} + M_c) = \mu_c H_{i,\mathrm{total}} \tag{A13}$$

and Eqs. A9 and A11, the demagnetizing factor becomes

$$\alpha = \frac{\mu_c - \mu_o}{\mu_c + \mu_o}, \tag{A14}$$

in agreement with Eq. 4. Finally, it is also easy to show that the magnetic potential outside the wire (that is, Eq. 3b) leads to the same expression of the magnetic force in Eq. 1.

Manuscript received Feb. 2, 2000, and revision received July 31, 2000.